# A new bearing fault diagnosis approach based on common spatial pattern features

## Ortak uzamsal örüntü özniteliklerine dayalı yeni bir rulman arızası teşhisi yaklaşımı

**Nurhan Gürsel Özmen[1]** (ID)**, Yunus Emre Karabacak[2],*** (ID)

*[1,2] Karadeniz Technical University, Department of Mechanical Engineering, 61080, Trabzon, Türkiye*

**Abstract**

Condition monitoring in machines holds significant importance for early fault detection, optimizing maintenance processes, and ensuring operational continuity. In this study, a novel intelligent detection approach for rolling bearings is introduced, utilizing the Common Spatial Pattern (CSP) method to extract distinctive features related to bearing faults. By maximizing the variance ratio of signal matrices from distinct sources, CSP sets itself apart from conventional frequency-based features. This technique captures characteristic vibration patterns unique to each measurement, enabling differentiation between faulty and healthy bearings. The effectiveness of the proposed method was assessed using Artificial Neural Network (ANN), Support Vector Machine (SVM), and K-Nearest Neighbour (k-NN) algorithms across two diverse datasets. The results indicated an 88.5% accuracy in two-class fault detection and 93.5% in fault classification when employing ANN. Comparison with traditional time domain feature sets highlighted the superior performance of CSP features, exhibiting elevated accuracy rates in both two-class and multiclass scenarios. Thus, CSP features emerge as a promising avenue for effectively monitoring bearing conditions through vibration data.

**Keywords:** Common spatial pattern, Bearings, Condition monitoring, Vibration signals

**Öz**

Makinelerde durum izleme, erken arıza tespiti, bakım süreçlerinin optimize edilmesi ve iş sürekliliğinin sağlanması açısından büyük öneme sahiptir. Bu çalışmada, rulmanlar için yeni bir akıllı tespit yaklaşımı sunulmuş, rulman arızalarıyla ilgili ayırt edici öznitelikleri çıkarmak için Ortak Uzamsal Örüntü (OUÖ) yöntemi kullanılmıştır. Farklı kaynaklardan gelen sinyal matrislerinin varyans oranını maksimize eden OUÖ, geleneksel frekans temelli özniteliklerden ayrılır. Bu teknik, her ölçümde benzersiz titreşim desenlerini yakalayarak arızalı ve sağlam rulmanlar arasındaki farkı belirlemeyi sağlar. Önerilen yöntemin etkinliği Yapay Sinir Ağı (YSA), Destek Vektör Makinesi (DVM) ve K-En Yakın Komşu (k-YK) algoritmaları kullanılarak iki farklı veri kümesinde değerlendirildi. Sonuçlar, YSA kullanıldığında iki sınıflı arıza tespitinde %88.5 doğruluk ve arıza sınıflandırmasında %93.5 doğruluk elde edilebileceğini gösterdi. Geleneksel zaman alanı öznitelikleri ile yapılan karşılaştırma, OUÖ özniteliklerinin üstün performansını ortaya koydu. OUÖ iki sınıflı ve çoklu sınıflı senaryolarda yüksek doğruluk oranları sergiledi. Böylece, OUÖ öznitelikleri titreşim verileri aracılığıyla rulman arızalarının etkili bir şekilde tespit edilmesi için umut verici bir yol olarak ortaya çıkmaktadır.

**Anahtar kelimeler:** Ortak uzamsal örüntü, Rulmanlar, Durum izleme, Titreşim sinyalleri

## 1 Introduction

Bearings are basic machine elements commonly used in rotating machinery such as in aviation, turbines, agricultural equipment, and motor vehicles. They can carry high dynamic loads that occur during the operation of the machines and are transmitted around the rolling element bearings [1]. Therefore, any failure in a bearing can cause serious problems that may lead to production deficiency and financial loss. Bearings often operate for long hours in harsh environments and frequently lose performance or break down [2]. It has been highlighted that a considerable portion of breakdowns in rotating machines is attributed to faulty bearings [3]. Hence, it is very important to study the condition monitoring of bearings for reducing operating costs and preventing industrial accidents.

Bearings produce noise and vibration due to their changing working conditions or due to any damage to the body. The radial loading of bearings may cause vibration even when they are geometrically perfect [4]. The oscillations may increase due to a defect [5]. In the rotating machinery industry, a vast number of condition-based strategies have been invented to describe the occurrence of faults [6]. The signal characteristics of a faulty bearing are generally non-stationary and multi-component which makes it difficult to identify from the raw signal accurately. Various techniques have been improved to detect failures in bearings [7].

In recent years, the analysis of vibration signals has become one of the most preferred and efficient methods used for detecting faults in bearings [8]. A large number of

diagnosis strategies have been recommended for vibration signal analysis [9], combining various feature extraction and classification methods for machine faults [10]. Feature extraction is considered the main distinguishing point in bearing fault diagnosis which is a crucial step for time domain, frequency domain, or both domains data by removing the noise and gathering the subject-specific information. Various methods, such as wavelet denoising [11], empirical mode decomposition [12], and time-frequency manifolds [13], have already been used to filter the noise and obtain satisfactory results. Among them, the wavelet denoising method is more efficient and usable. In frequency domain analysis [14], the repetition frequencies of the impulse response series, which arise both from the passage of the fault in and out of the load zone are observed by several mathematical methods. Among them, the spectral representation of signals and the Fourier transform are the most preferred, easy-to-apply algorithms [15]. Moreover, Kalman filtering [16], the spectrogram [17], empirical mode decomposition [18], multiscale permutation entropy [19], the envelope spectrum [20], the adaptive spectral kurtosis [21], the cyclic spectral correlation and coherence [22] and the negentropy [23] are some of the other commonly used algorithms. The defect frequency extraction is not very efficient in rolling bearings with a low signal-noise ratio (SNR). It is stated that the impulse energy of the defective bearing is kept in the machine noise and the fault frequency can not be observed in the envelope spectrum [24]. In this case, besides the frequency range of the impact location, the exact time of emergence of the impact is also necessary. Therefore, time-frequency analysis like wavelet transform [25] and its combinations with envelope spectrum [26], multi-scale morphological filters [27], adaptive mode decomposition [28], multiscale complexity analysis [29], autoregressive model [30] and Wigner-Ville analysis [31] are the other methods that were used. However, if the fault signals are weak, these methods may not work.

Since the signal characteristics and the processing methods have much in common, feature extraction techniques used in biomedical signal analysis have found themselves a way into rotating machinery analysis. Therefore, we proposed the Common Spatial Pattern (CSP) method, which is considered a powerful feature extraction method in the electroencephalogram (EEG) processing for Brain-Computer Interfaces (BCI) for the vibration data of bearings [32]. The method of common spatial patterns (CSP) implements spatial filters by computing the variances in the filtered time series for optimal discrimination [33]. Spatial filtering can significantly enhance the discrimination ability while separating the signal from the noise. In a recent study by Karabacak and Özmen [34], CSP has become successful in diagnosing the faults of worm gearboxes under different working conditions. In a study by Li et al. [35], a variational mode decomposition and high dimensional Common Spatial Pattern-based feature extraction are utilized for rolling bearings.

Although bearing diagnostics are widely studied and many methods have been developed for them, due to the improvements in the feature extraction of various signals,

new methods are being introduced to the condition monitoring of bearings. In this study, we have tested the CSP method on the Case Western Reserve University (CWRU) Bearing Data [36,37] and the University of Ferrara, Italy, Engineering Department Data [38], to classify healthy and faulty bearings. ANN, SVM, and k-NN are used to train CSP features and then to classify the faults [39]. The results of the study were given comparatively by accuracy metrics. The results of the study were given comparatively by SVM and k-NN by accuracy metrics. Furthermore, classical time domain features and the high distinguishing capability of the CSP features were compared and the results are presented.

Support Vector Machine (SVM), Naive Bayes, K-Nearest Neighbor (k-NN), Random Forest, Decision Trees, and Deep Learning methods are the frequently used machine learning algorithms in fault detection of machinery [40]. The superiority of Artificial Neural Networks (ANN) and SVM has been proven in rotating machines [41]. Newly, Deep Learning (DL) based solutions like Convolutional Neural Networks (CNNs) have also been tried for fault diagnosis of bearings [42]. Deep learning and ensemble learning techniques have some limitations. A reasonable amount of data gathering and complex analyzing methods with their tuning is still a problem to handle which can be handled in future studies [43].

In the study by Zhao et al. [44], bearing fault diagnosis was performed using transfer learning and an optimized deep belief network. The effectiveness of the proposed approach was validated using vibration data from a rotating machinery. In the research conducted by Kaya et al. [45], they introduced a novel approach for feature extraction in bearing fault classification. Their method involved utilizing one-dimensional gray-level co-occurrence matrices. Upon subjecting the signals to their proposed model, the achieved success rates were notably high across various datasets. In the study conducted by Bayram et al. [46], the impact of bearing faults on coefficients obtained through wavelet transform was investigated. Through a series of experimental studies, it was concluded that the approach reliant on wavelet transform coefficients effectively achieves the classification of distinct types of bearing faults. In their study, Kaya et al [47]. introduced a novel method for automated diagnosis of bearing fault sizes. This method involves the utilization of time-frequency images generated through Continuous Wavelet Transform (CWT), coupled with deep transfer learning techniques. In his research, Kuncan [48] presented an intelligent methodology for bearing fault diagnosis that involves the integration of two distinct techniques: one-dimensional local binary pattern analysis and gray relational analysis. In the study conducted by Yang et al. [49], the focus was on the interpretability of deep convolutional neural networks (CNNs) in the context of rolling bearing fault diagnosis.

Up to now, many methods have been presented for condition monitoring some of which were for constant operational conditions and therefore do not represent the real working conditions in industrial applications [50]. In [51], it is stated that there is a need for a benchmark study that applies novel diagnostic algorithms and they have presented

some solid results. They suggested that the researchers propose novel methods and propose the superiority of their algorithm against the Randall results or similar results with cost-effective methods. Therefore, in this study, we used the Common Spatial Pattern method as a new diagnosing tool to distinguish bearing faults, which is a powerful feature extraction technique in EEG signal processing. To give a better diagnosis for datasets, the CSP-based approach can overcome the confusion created by the nonlinearity and the inadequacy of classical methods such as statistical features and envelope analysis. Moreover, it is computationally simple and efficient. The study is unique in its use of CSP features for the fault detection of bearings and performing a remarkable classification performance when compared to the state-of-the-art methods.

The remainder of this paper is presented in the following manner. In Section 2, the data sets are introduced and the theoretical background of CSP is given. Section 3 presents the results of both data sets with the proposed models. The Conclusions are given in the final chapter Section 4.

## 2 Materials and methods

### 2.1 The ball bearing and its geometry

Bearings are precision-manufactured machine elements that enable machines to work efficiently at high speeds and to carry heavy loads safely. As there are balls placed between the inner and outer races of rolling elements, they can carry axial or radial loads with minimum torsional friction. Deep groove ball bearings are the simplest type of bearings commonly used in industry. The main parts of the ball bearings such as the inner, and outer races, balls, the cage, and the shaft are given in Figure 1 [52].
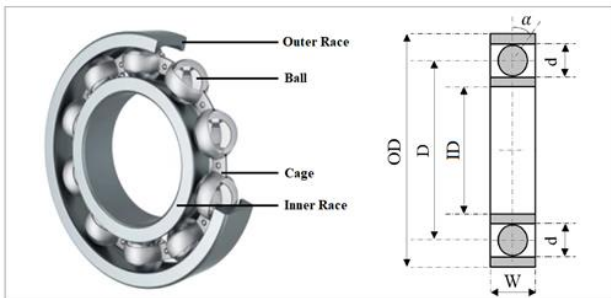


**Figure 1.** Fundamental dimensions of Deep-groove bearing (OD: outer race diameter; D: pitch diameter; ID: inner diameter or bore diameter; d: rolling element diameter, W: raceway width, α: contact angle [52]

During the rotation of a ball bearing, the outer race is fixed while the inner race and balls move. The correct alignment and placement are very important for the maximum lifespan of this equipment, if not, several kinds of defects can occur such as cracks or pits on moving surfaces or bearing elements, or other harms such as roughness or misaligned races may occur. The cracks or pits may be observed on the inside of the outer race such that is forced with higher loads. On the other hand, the inner race faults can be observed at any point of the race due to rotation.

### 2.2 The Case Western Reserve University dataset (CWRU)

In this study, we used the Case Western Reserve University (CWRU) vibration data [51]. In Figure 2 the test system is shown which has a 2 hp Reliance Electric motor with a torque sensor and encoder fixed on it. Torque is supplied from a dynamometer and an electronic control unit. The CWRU Bearing Data Center website has details about the test system [36].
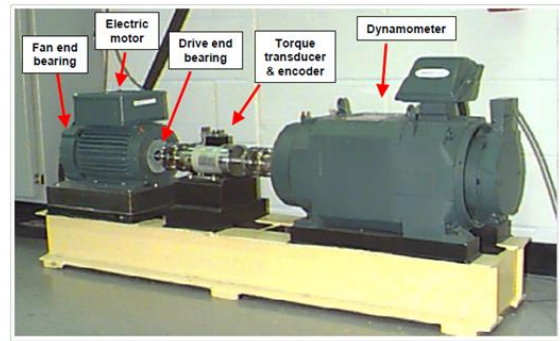


**Figure 2.** The bearing test rig [51]

The data were obtained for many different conditions and 161 datasets were formed. We used the dataset from Table 3, 48k drive end bearing fault data with 48 kHz sampling frequency, containing 1 healthy and 3 defective bearings (6203-2RS). They are denoted as HB (healthy bearing), FB1 (bearing with outer race fault), FB2 (bearing with inner race fault), and FB3 (bearing with rolling element fault). The speed of the shaft in the experimental setup was approximately 6 Hz for all signals, and the sampling frequency was 48000 samples/s. The signal length is 200000 samples for each bearing [51]. Table 1 shows the fundamental specifications of the bearings.

A reasonable amount of vibration can be observed in ball bearings; even if they are perfectly aligned and fixed. The vibration level may increase if there is any fault in one of the elements of the ball bearing. Figure 3 shows common bearing faults.
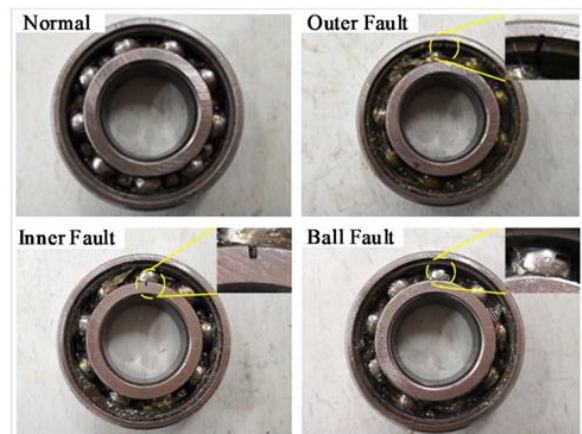


**Figure 3.** Pictures of HB (healthy bearing), FB1 (bearing with outer race fault), FB2 (bearing with inner race fault), and FB3 (bearing with rolling element fault) [42]

**Table 1.** Fundamental dimensions of the test bearings [51]

| Symbol | Explanation | Value |
|--------|-------------|-------|
| D | Pitch diameter | 38.5 [mm] |
| ID | Inner diameter | 25 [mm] |
| OD | Outer race diameter | 52 [mm] |
| d | Rolling element diameter | 7.12 [mm] |
| W | Raceway width | 15 [mm] |
| $n$ | The rolling element number | 12 [-] |
| $\alpha$ | The angle of contact | 0 [°] |

## 2.3 The University of Ferrara dataset

The second data set is from the The University of Ferrara, Department of Engineering from Italy [38]. This dataset comprises the vibration data obtained throughout a test study on bearings defined by artificial faults on the outer ring. Vibration signals were obtained for several working statuses. These were described by various values of implemented load, shaft rotation speed, and fault size. The test rig is given in Figure 4. The bearing faults utilized in the experiments can be seen schematically in Figure 5. The test bearing is mounted on the shaft end and enclosed in a housing. Apart from the test bearing, two bearings are utilized as supporting bearings. There is a coupling between the support bearings and the electric motor. An inverter controls the speed of the electric motor. Different loads can be implemented to the test bearing in the vertical direction. The acceleration signals are obtained using a data collection system and a sensor mounted on the test bearing [38].
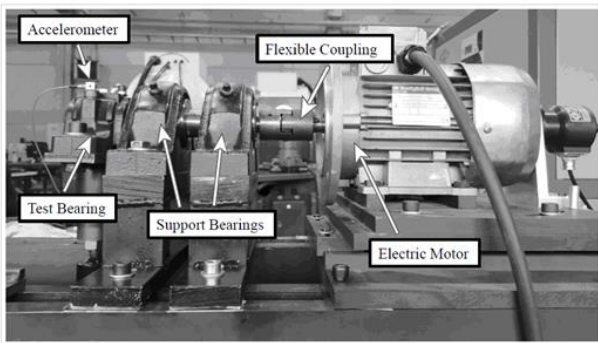


**Figure 4.** The University of Ferrara bearing test rig [38]
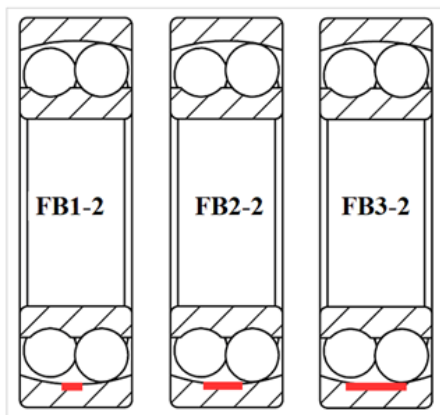


**Figure 5.** The University of Ferrara dataset fault types

Bearings with different fault sizes (FB1-2, FB2-2, and FB3-2) were tested under various combinations of applied loads and shaft rotational speeds, and vibration data were collected. Faults in the outer ring of the bearings were artificially made by the electric discharge process. The sampling frequency of each signal is 51.2 kHz and the measurement time is 15 s [38].

## 2.4 Methodology

The data sets are evaluated separately. According to the flowchart in Figure 6, the raw data is preprocessed then the feature extraction is applied. After that, the feature sets are sent to the classifiers in order to detect healthy and faulty bearings with different defect types.
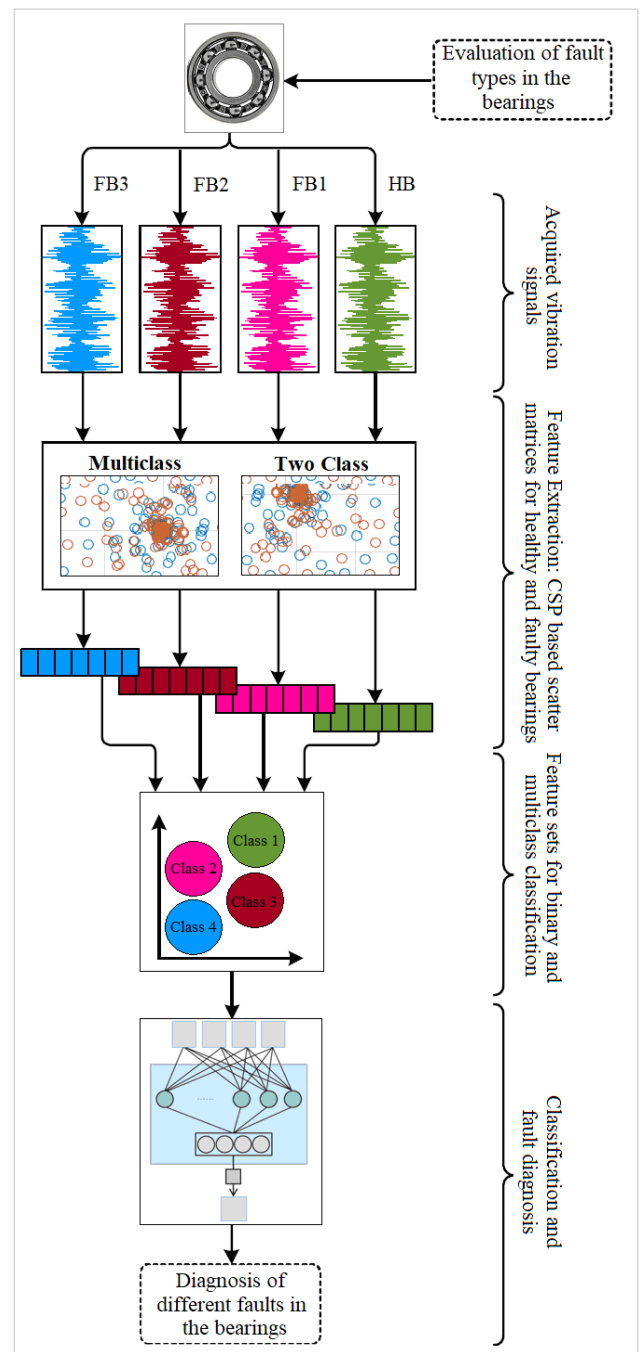


**Figure 6.** The bearing fault detection flowchart

### 2.4.1 Feature extraction with Common Spatial Pattern (CSP)

In signal processing, the CSP method separates a multivariate signal with maximum distinctions in variance between two windows. It is efficiently used in maximizing the variance ratio of the two-class signal matrices in EEG signal processing and it can be applied to two or multi-class classification problems. If $X_1$ and $X_2$ are the estimates of the covariance matrices of classes 1 and 2 respectively, then the CSP algorithm uses the simultaneous diagonalization of two covariance matrices ($X_1$, $X_2$). This can be implemented mathematically by solving the eigenvalue decomposition problem [53].

In Equation (1), $P$ is the CSP projection matrix ($P \in R^{NXN}$), and it obtains the features whose variances are best for classifying two classes of signals. The rows of $P$ are fixed spatial filters, and CSP can be calculated from rows of $P^{-1}$. $D$ is a diagonal matrix and involves the eigenvalues of $X_1$. For each $j^{th}$ attempt of the vibration signal, $V_j \in R^{NXT}$ is converted into a low-dimensional subspace with the projection matrix ($P$). Here, $V_j$ is the matrix composed of vectors of vibration signals. Besides, $N$ denotes the number of vibration signals and $T$ represents the number of samples per trial. In Equation (2), the linear transformation of the $j^{th}$ trial is given. Here $S_j \in R^{NXT}$ is used to show the spatially filtered data, and these signals maximize the difference in the variance of two classes of vibration data [53].

$$X_1 P = (X_1 + X_2)PD \qquad (1)$$

$$S_j = PV_j \qquad (2)$$

The subsets of the data are selected from the $n$ pairs of the first and last rows of $S_j$. If $S_f \in R^{2nxT}$ are the first and last rows of $S_j$, then the variance of $S_f$ forms the feature vector for the $j^{th}$ trial. Accordingly, $f_j$ can be written as in Equation (3) ($n = 2$ and $f_j \in R^{2n}$). Here, $f_j$ denotes the two-class features for one class versus another class for the $j^{th}$ trial [53].

$$f_j = \log\left[\frac{\text{var}(S_f)}{\sum_{j=1}^{2n} \text{var}(S_f)}\right] \qquad (3)$$

Figure 7 shows the distribution of samples of two classes before and after CSP filtering. The red and blue circles are plotted from Gaussian distributions of healthy and faulty bearing sets. In (a), the distribution of prefiltering is shown. In (b), the distribution after the filtering is given. The samples in Figure 7(a) are mapped to the ones in Figure 7(b) by CSP where the two distributions are completely different

along the new axes. The estimated covariances show the direction of CSP projections. It is clear that the two classes are independent of each other, that is, they are different classes. Therefore, the horizontal (vertical) axis represents the highest variance in the red (blue) class and oppositely the smallest in the blue (red) class [54].
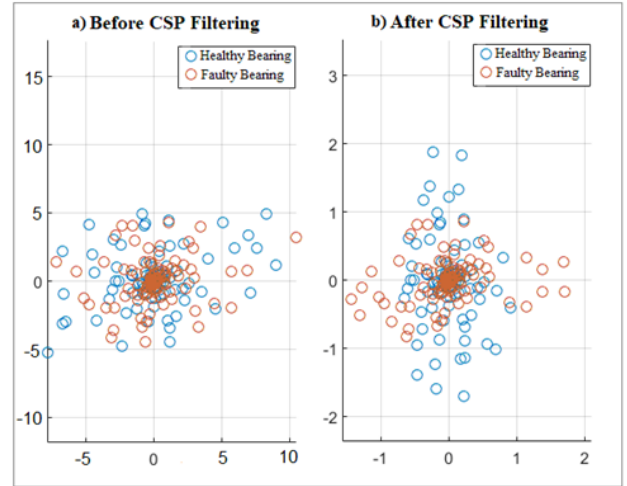


**Figure 7.** (a) Distribution of vibration data before CSP filtering (b) Distribution of vibration data after CSP filtering

### 2.4.2 Fault detection

After the 2000s, ANN has become a superb machine learning technique. It is commonly applied to many engineering problems from modeling to classification. There are many studies in the literature on the condition monitoring of rotary machines and bearing fault detection [55].

A representative ANN is shown in Figure 8 containing two hidden layers. The parameters, $x_1$, $x_2$ and $x_3$ represent the inputs, and $y$ represents the output. A mathematical function is defined as in Equation (4) for the relation between the output and inputs. $f$ is the activation function of the network, and $b$ is a fixed quantity. The classifier parameter or weight is shown by $W$ produced after an iterative training process [43].

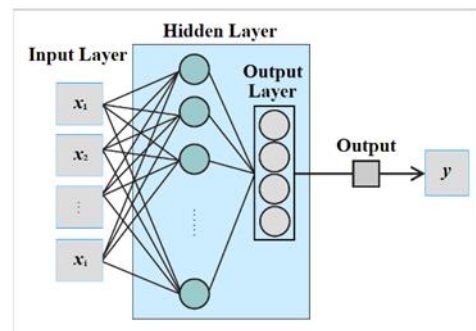$$y = f(W^T x) = f\left(\sum_{i=1}^{3} W_i x_i + b\right) \qquad (4)$$



**Figure 8.** Two hidden layers of the ANN

The dataset containing vibration data CSP features is used in the detection of bearing faults with two-class or multi-class ANN classifiers. For this purpose, the binary classification contains six pairs where the ANN outputs are labeled as healthy and faulty bearing pairs (Table 2). The datasets are partitioned as 70% training, 15% validation, and 15% test. In multiple classifications, the one versus rest-voting strategy is used to obtain the four classes of all bearing types (Table 2).

**Table 2.** Binary and multiclass CSP pairs for machine learning algorithms

| CWRU Two-class Classification Pairs | HB vs FB1 | HB vs FB2 | HB vs FB3 | FB1 vs FB2 | FB1 vs FB3 | FB2 vs FB3 |
|---|---|---|---|---|---|---|
| The University of Ferrara Two-class Classification Pairs | FB1-2 vs FB2-2 | | FB1-2 vs FB3-2 | | FB2-2 vs FB3-2 | |
| CWRU Multiclass Classification | HB | | FB1, FB2, FB3 | | | |
| | FB1 | | HB, FB2, FB3 | | | |
| | FB2 | | HB, FB1, FB3 | | | |
| | FB3 | | HB, FB1, FB2 | | | |
| The University of Ferrara Multiclass Classification Pairs | FB1-2 | | FB2-2, FB3-2 | | | |
| | FB2-2 | | FB1-2, FB3-2 | | | |
| | FB3-2 | | FB1-2, FB2-2 | | | |

We used a feedforward ANN algorithm with a hidden and output layer both binary and multiple classification processes. In most ANN problems, using a single hidden layer is usually sufficient to solve the problem. There is no general rule in determining the number of neurons in the hidden layer. If the number of neurons in the hidden layer is chosen too small, the classification success will be low. Using a large number of neurons in the hidden layer can result in longer training time and overfitting. Accordingly, in order to designate the optimal number of neurons in the hidden layer, the dimensions of the input and output layers should be chosen by considering them. After some trials, the feasible artificial neuron numbers in the hidden layer were chosen as 20. We utilized the log-sigmoid transfer function as it is suitable and preferred for small networks.

SVM is a well-known supervised method that creates a hyperplane between different datasets and classifies two classes of data. SVM moves the problem to a higher dimensional space using a suitable kernel function, and it solves complex and multidimensional problems [56]. K-NN non-parametric supervised learning method which is used mostly for classification and regression. The output of k-NN is a class membership where the class label of a new sample is attained by the class label of its $k$ nearest neighbors [57]. The Euclidean distance is the most commonly used metric.

### 2.4.3 Classification evaluation criteria

The toolboxes in Matlab R2021a software were used for ANN, SVM, and k-NN applications in this study. Accuracy, precision, sensitivity, and specificity were chosen as performance metrics [58].

All the calculations are performed with MATLAB R2021a, on a PC with a 2.4-GHz CPU and 16 GB RAM. The average computation time is around 2 s to analyze the samples in 4 or 3 classes, showing that the recommended method is computationally capable.

## 3 Results and discussion

### 3.1 Case 1: CWRU dataset

Vibration data obtained from four different bearing sets HB, FB1, FB2, and FB3 were preprocessed and the feature sets were formed. The duration of each measurement is 4.16 s, and the sampling frequency is 48000 samples/s. The signal length is 200000 samples for each bearing. In Figure 9, time-domain vibration signals are given. The vibration amplitudes of the HB bearing are lower than the other bearings. The highest amplitudes were observed in the FB1 bearing. Moreover, periodic sharp peaks are more frequent in FB1 and FB2 due to the faults.
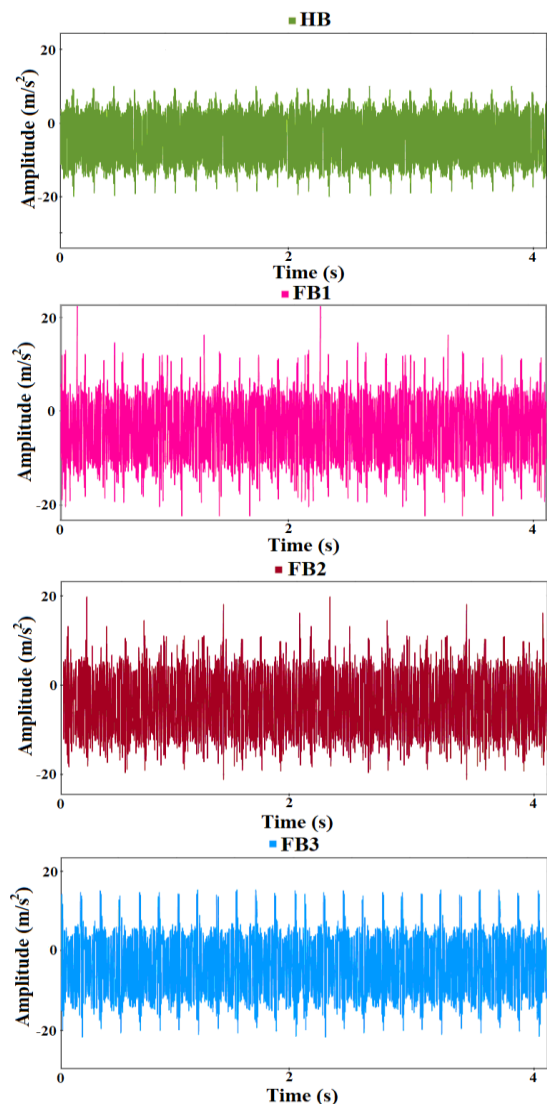


**Figure 9.** CWRU Raw vibration signals in the time domain

In Figure 10, frequency domain power spectrums of the bearing signals are given. Since the power spectrums seem similar, further spectral calculations are needed to comment on this situation.
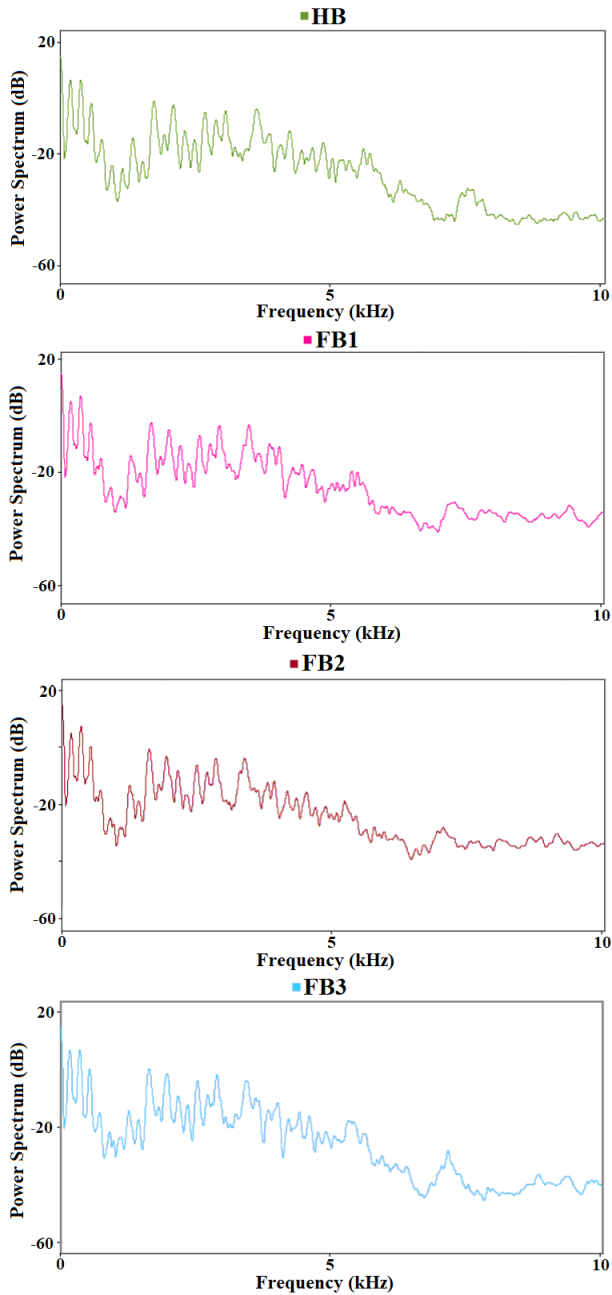
**Figure 10.** CWRU Power spectrum of the vibration signals

### 3.1.1 CSP-based Two-class ANN classification results

In Figure 11, the scatter matrices of CSP features for all defined bearing pairs are given. In Table 3 and Figure 12, performance comparisons of CSP-based binary ANNs are presented for healthy and faulty bearings. It can be observed from Table 3 that, the highest classification accuracy (88.5 %) is obtained for healthy bearing (HB) and bearing with outer race fault (FB1). Although the lowest accuracy (81.5%) was observed between bearing with outer race fault (FB1) and bearing with rolling element fault (FB3), it is notable that the value is considerably high. These results can also be inferred from the scatter plots of CSP features in Figure 11.
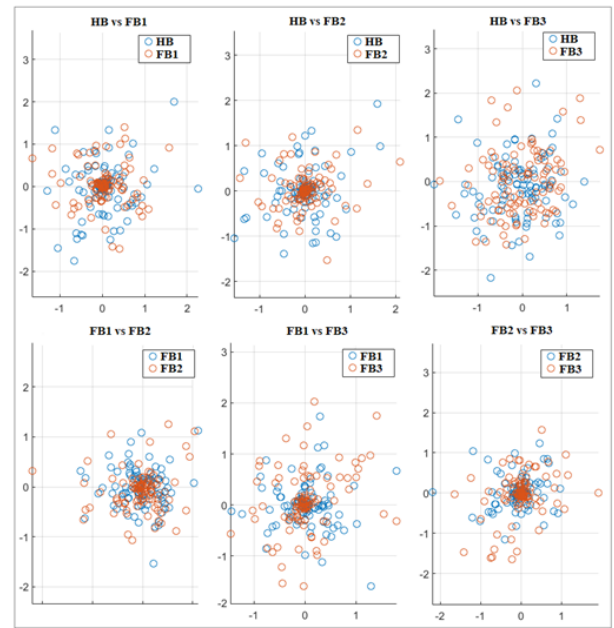


**Figure 11.** CSP feature visualization of CWRU Data

**Table 3.** CSP-based binary ANN accuracy results

| CSP-based Two-class Classification | | | | |
|---|---|---|---|---|
| Bearing Pairs | Accuracy | Precision | Sensitivity | Specificity |
| HB vs FB1 | 0.885 | 0.920 | 0.859 | 0.913 |
| **HB vs FB2** | **0.880** | **0.960** | **0.828** | **0.952** |
| HB vs FB3 | 0.835 | 0.910 | 0.791 | 0.894 |
| FB1 vs FB2 | 0.835 | 0.770 | 0.885 | 0.796 |
| FB1 vs FB3 | 0.815 | 0.800 | 0.825 | 0.806 |
| FB2 vs FB3 | 0.820 | 0.710 | 0.910 | 0.762 |
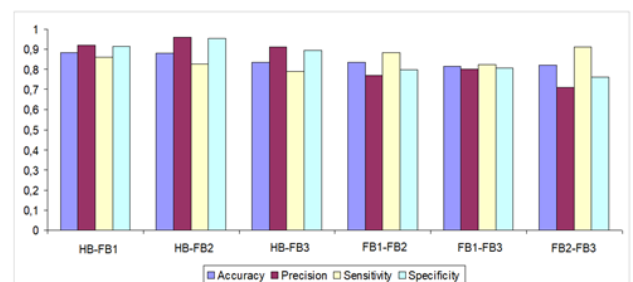


**Figure 12.** Bar graphs for accuracy metrics of ANN

### 3.1.2 Multiclass ANN classification with CSP

The performance for a single fault and all other faults are represented in this section respectively. In Figure 13, the scatter plots of four different cases are given. Table 4, and Figure 14 show performance metrics such as accuracy, precision, sensitivity, and specificity values of CSP-based multiclass ANN classifiers, for fault diagnosis in bearings. The results of multiclass classification for bearings are remarkably high enough and depicted as bold in tables. Therefore, we can conclude that the CSP values of HB and the rest have the highest distinctiveness (93.5 accuracy, 1 precision, 88.5% sensitivity, and 1 specificity).
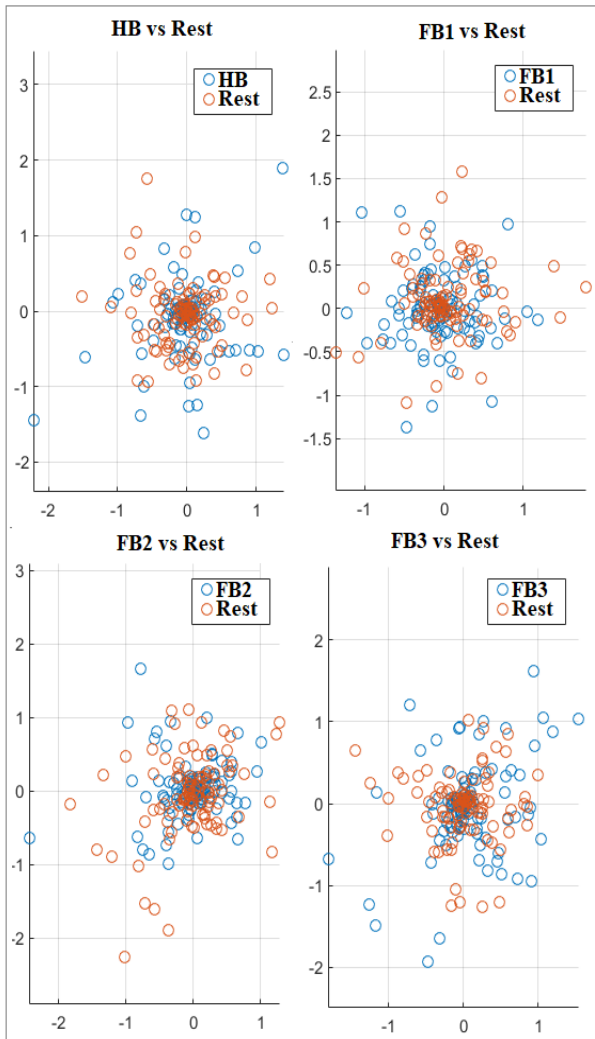
**Figure 13.** CSP feature visualization for all fault types

**Table 4.** Performance metrics for CSP-based ANN fault classification

| Bearing Pairs | Accuracy | Precision | Sensitivity | Specificity |
|---|---|---|---|---|
| **HB vs Rest** | **0.935** | **1** | **0.885** | **1** |
| FB1 vs Rest | 0.880 | 0.950 | 0.833 | 0.942 |
| FB2 vs Rest | 0.870 | 0.860 | 0.878 | 0.863 |
| FB3 vs Rest | 0.915 | 0.960 | 0.881 | 0.956 |

When the binary and multiple classification results are examined, it is seen that the classification accuracies are high enough to be declared. Moreover, bearing with rolling element fault (FB3) is considered the most difficult fault that can be diagnosed [51]. In general, the amplitudes of the frequency components of the ball passing from the outer and inner race are higher, while the amplitudes of frequency components of the ball spin are less. Therefore, the detection of the FB3 fault is also more difficult. However, in our study, 93.5 % accuracy for HB-FB3 and 91.5% for multiclass FB3 and Rest classification were obtained.
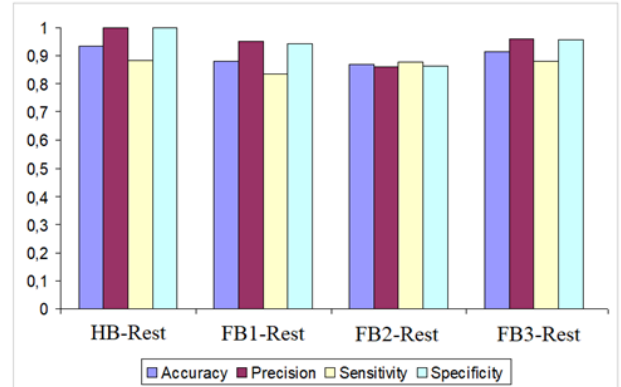


**Figure 14.** Bar graphs for accuracy metrics of CSP-based multiclass ANN

### 3.1.3 Classifier comparison between ANN -SVM - k-NN

In this part of the study, SVM and k-NN results for binary and multiclass classification are given comparatively to show the efficiency of similar classifiers that are usually preferred for vibration data fault detection. A standard type k-NN and a Gaussian kernel type SVM were tried. In Table 5 and Figure 15, all of the performance metrics are presented. From the tables, it is clear that ANN outperforms SVM and the k-NN (88.5% ANN, 66% SVM, and 50.5% k-NN). It is stated that k-NN performs well when the sample size is small; it is very simple and requires tuning only one hyperparameter (the value of k).

**Table 5.** Performances of different classifiers

| | ANN | SVM | k-NN |
|---|---|---|---|
| **HB vs FB1** | **0.885** | 0.660 | 0.505 |
| HB vs FB2 | 0.880 | 0.685 | 0.520 |
| HB vs FB3 | 0.835 | 0.755 | 0.505 |
| FB1 vs FB2 | 0.835 | 0.615 | 0.520 |
| FB1 vs FB3 | 0.815 | 0.650 | 0.505 |
| FB2 vs FB3 | 0.820 | 0.655 | 0.510 |
| **HB vs Rest** | **0.935** | 0.795 | 0.785 |
| FB1 vs Rest | 0.880 | 0.825 | 0.755 |
| FB2 vs Rest | 0.870 | 0.805 | 0.575 |
| FB3 vs Rest | 0.915 | 0.810 | 0.835 |
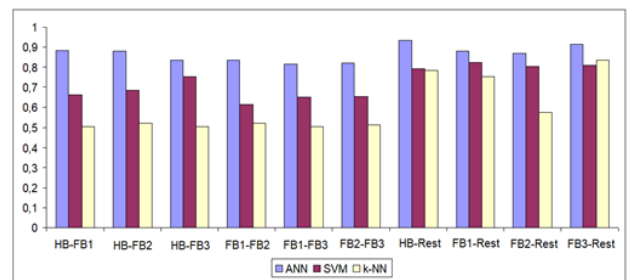


**Figure 15.** Bar graph comparisons for various classifiers

When the data size is larger, SVM and ANN are preferred. Although SVM is a powerful classification method, for this vibration data, we have obtained higher accuracies with ANN. There can be several possible explanations for this result; deep architectures can represent intelligent behavior more efficiently than shallow architectures like SVMs, in an ANN there are a bunch of hidden layers with fixed sizes depending on the number of

features. Parametric models represent them whereas SVMs are non-parametric [59].

### 3.1.4 Evaluation of CSP features versus Classical Statistical Features (CSF)

To demonstrate the effectiveness and distinctiveness of CSP features, we compared CSP results with generally used time domain statistical features (CSF) like standard deviation (SD), Root mean square (RMS), variance (VAR), kurtosis (K) and skewness (SK) [60]. These features were calculated and fed to the ANN classifiers. The results are shown in Table 6. From the table, it can be seen that using CSP features has achieved higher accuracies in all two-class and multiclass cases. Therefore, we can conclude that in condition monitoring of bearings, CSP features will be a possible tool in fault detection to improve diagnostic performance. In addition, CSP can reduce time and calculation energy loss due to complex and high-dimensional CSF calculations.

**Table 6.** Comparison of CSP and CSF features

|  | CSP-ANN | CSF-ANN |
|---|---|---|
| **HB vs FB1** | **0.885** | 0.860 |
| HB vs FB2 | 0.880 | 0.820 |
| HB vs FB3 | 0.835 | 0.830 |
| FB1 vs FB2 | 0.835 | 0.830 |
| FB1 vs FB3 | 0.815 | 0.800 |
| FB2 vs FB3 | 0.820 | 0.800 |
| **HB vs Rest** | **0.935** | 0.900 |
| FB1 vs Rest | 0.880 | 0.850 |
| FB2 vs Rest | 0.870 | 0.860 |
| FB3 vs Rest | 0.915 | 0.900 |

### 3.2 Case 2: The University of Ferrara dataset signal analysis

Time domain vibration signals and frequency domain power spectrums of the four different bearing sets FB1-2, FB2-2, and FB3-2 are given in Figure 16.
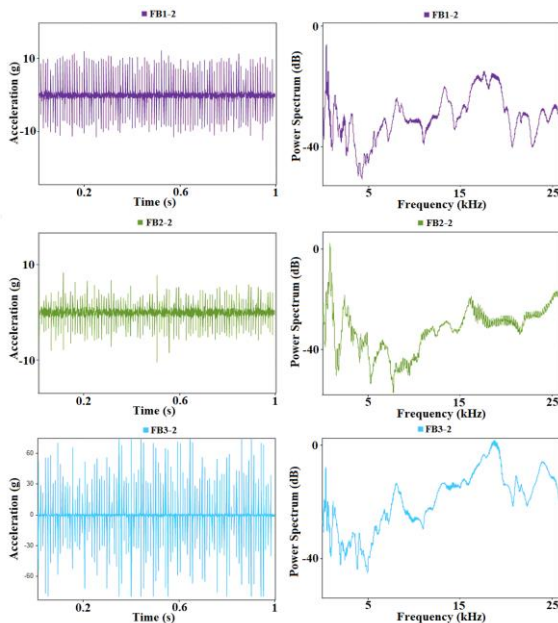


**Figure 16.** The vibration signals in the time and frequency domain

### 3.2.1 CSP-based Two-class ANN classification for the second dataset

In Figure 17, the scatter matrices of CSP features for the second dataset are given. In Table 7 performance comparisons of CSP-based binary ANNs are given for faulty bearings.
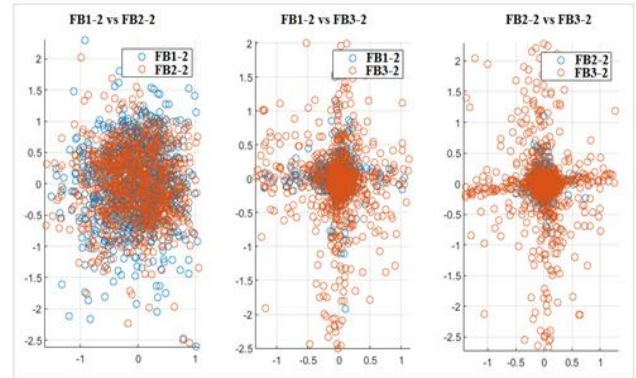


**Figure 17.** CSP projections of acceleration data for two-class ANN for the second dataset

**Table 7.** CSP-based binary ANN accuracy results

| CSP-based Two-class Classification | | | | |
|---|---|---|---|---|
| Bearing Pairs | Accuracy | Precision | Sensitivity | Specificity |
| FB1-2 vs FB2-2 | 0.750 | 0.800 | 0.714 | 0.800 |
| FB1-2 vs FB3-2 | 0.833 | 0.667 | 1 | 0.750 |
| **FB2-2 vs FB3-2** | **0.917** | **0.833** | **1** | **0.857** |

### 3.2.2 The University of Ferrara multiclass ANN classification with CSP

The performance for a single fault and all other faults are represented in this section respectively. In Figure 18, the scatter plots of 3 different cases are given. Table 8, shows performance metrics such as accuracy, precision, sensitivity, and specificity values of CSP-based multiclass ANN classifiers, for the second dataset.
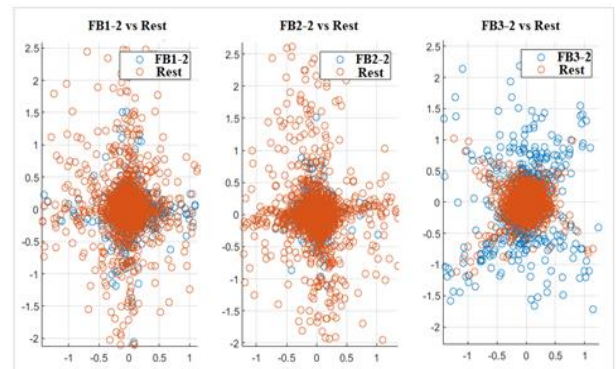


**Figure 18.** CSP features separation for all fault types

**Table 8.** Performance metrics for CSP-based ANN fault classification for the second dataset

| Bearing Pairs | Accuracy | Precision | Sensitivity | Specificity |
|---|---|---|---|---|
| FB1-2 vs Rest | 0.917 | 0.833 | 1 | 0.857 |
| FB2-2 vs Rest | 0.833 | 0.667 | 1 | 0.750 |
| **FB3-2 vs Rest** | **0.917** | **1** | **0.857** | **1** |

### 3.2.3 Classifier comparison between ANN -SVM - k-NN

In this part of the study, SVM and k-NN results for binary and multiclass classification are given for the second dataset. In Table 9 all of the performance metrics are presented.

**Table 9.** Performances of different classifiers

| | ANN | SVM | k-NN |
|---|---|---|---|
| FB1-2 vs FB2-2 | 0.750 | 0.833 | 0.510 |
| FB1-2 vs FB3-2 | 0.833 | 0.917 | 0.667 |
| **FB2-2 vs FB3-2** | **0.917** | **0.917** | 0.583 |
| FB1-2 vs Rest | 0.917 | 0.833 | 0.583 |
| FB2-2 vs Rest | 0.833 | 0.917 | 0.510 |
| FB3-2 vs Rest | 0.917 | 0.750 | 0.417 |

### 3.2.4 Evaluation of CSP features versus Classical Statistical Features (CSF) for the second dataset

The results can be seen in Table 10. From the table, it is quite apparent that using CSP features has achieved higher accuracies in all two-class and multiclass cases for the second dataset.

**Table 10.** Comparison of CSP and CSF features

| | CSP-ANN | CSF-ANN |
|---|---|---|
| FB1 vs FB2 | 0.750 | 0.710 |
| FB1 vs FB3 | 0.833 | 0.750 |
| **FB2 vs FB3** | **0.917** | 0.850 |
| **FB1 vs Rest** | **0.917** | 0.850 |
| FB2 vs Rest | 0.833 | 0.800 |
| **FB3 vs Rest** | **0.917** | 0.850 |

### 3.3 Comparison of CSP-based ANN performance with the existing literature

CWRU bearing diagnostic vibration data [36] were commonly used in the literature as it's a benchmark dataset. In this part of the study, we have compared our results with the existing literature that they have used a similar structure to our dataset. Although many studies have used CWRU data, the selected working datasets and the methodologies differ in concept. Therefore, it is difficult to make a logical comparison between these studies. In the study by Sun, J. et al. [61], they proposed a novel method for bearing fault detection, coming from the idea of compressed sensing and deep learning. Table 11 compares the average accuracy

results obtained with the methods used in this study with the results of [62,63].

**Table 11.** Comparison of the results with the existing literature

| Method | Average Accuracy |
|---|---|
| CSP-based SVM (CRWU) | 0.72 |
| CSP-based k-NN (CRWU) | 0.60 |
| CSP-based ANN(CRWU) | 0.88 |
| CSF-based ANN(CRWU) | 0.85 |
| CSP-based SVM (The University of Ferrara) | 0.86 |
| CSP-based k-NN (The University of Ferrara) | 0.55 |
| CSP-based ANN (The University of Ferrara) | 0.86 |
| CSF-based ANN (The University of Ferrara) | 0.80 |
| Compression sampling-based Deep Neural Networks [61] | 0.97 |
| Raw time domain signal-based Deep Neural Networks [62] | 0.96 |
| GoogleNet-CNN [63] | 1 |
| ResNet-50-CNN [63] | 1 |
| AlexNet-CNN [63] | 0.9 |
| EfficientNet-B0-CNN [63] | 1 |

The average accuracy obtained from the studies in [61-63] is higher than the accuracy rates obtained from the CSP-based diagnostics proposed in this study. However, considering the computational complexity and the applicability of the deep learning approach, CSP-based diagnostics can still yield satisfactory results for simplicity and rapid diagnosis.

## 4 Conclusions

A novel fault diagnosis method for rolling bearing via the CSP algorithm is recommended in this study. CSP maximizes the variance ratio of the two-class signal matrices coming from different sources. The case study is validated with two known data sets. It is proven with the calculations that the use of CSP features is both powerful and advantageous to identify different faults in terms of computational load. An 88.5% accuracy was obtained with ANN for two-class fault detection and 93.5% for fault classification. The results of the study were tested with SVM and k-NN, and it is seen that ANN has the highest accuracy performance. Moreover, classical time domain feature set results were also presented comparatively. CSP features have achieved higher accuracies in all two-class and multiclass cases. The proposed feature extraction method does not use the typical frequency or time domain features; instead, it focuses on capturing the covariance nature of impact vibrations. The CSP-based approach can overcome the confusion created by the nonlinearity and the inadequacy of classical methods such as statistical features and envelope analysis. We can propose CSP features to be used for condition monitoring of bearings with acceleration data. Based on the findings of this study, further research could explore the application of the CSP algorithm to a wider range of machinery and mechanical systems beyond rolling bearings, in order to determine its effectiveness in fault diagnosis across various industrial contexts.

**Conflict of interest**

The authors declare that there is no conflict of interest.

**Similarity rate (iThenticate):** %10

**References**

[1] J. Chen, C. Lin, D. Peng and H. Ge, Fault diagnosis of rotating machinery: A review and bibliometric analysis. Ieee Access, 8, 224985-225003, 2020. https://doi.org/10.1109/ACCESS.2020.3043743

[2] O. AlShorman, M. Irfan, N. Saad, D. Zhen, N. Haider, A. Glowacz and A. AlShorman, A review of artificial intelligence methods for condition monitoring and fault diagnosis of rolling element bearings for induction motor. Shock and vibration, ID 8843759, 2020. https://doi.org/10.1155/2020/8843759

[3] P. Bangalore and L.B. Tjernberg, An artificial neural network approach for early fault detection of gearbox bearings. IEEE Transactions on Smart Grid, 6(2), 980-987, 2015. https://doi.org/10.1109/TSG.2014.2386305

[4] P. Gupta and M.K. Pradhan, Fault detection analysis in rolling element bearing: A review. Materials Today: Proceedings, 4(2), 2085-2094, 2017. https://doi.org/10.1016/j.matpr.2017.02.054

[5] R. Yao, H. Jiang, Z. Wu and K. Wang, Periodicity-enhanced sparse representation for rolling bearing incipient fault detection. ISA transactions, 118, 219-237, 2021. https://doi.org/10.1016/j.isatra.2021.02.023

[6] S. Lu, P. Zhou, X. Wang, Y. Liu, F. Liu and J. Zhao, Condition monitoring and fault diagnosis of motor bearings using undersampled vibration signals from a wireless sensor network. Journal of Sound and Vibration, 414, 81-96, 2018. https://doi.org/10.1016/j.jsv.2017.11.007

[7] J. Wang, M. Xu, C. Zhang, B. Huang and F. Gu, Online bearing clearance monitoring based on an accurate vibration analysis. Energies, 13(2), 389, 2020. https://doi.org/10.3390/en13020389

[8] H.O. Omoregbee and P.S. Heyns, Fault classification of low-speed bearings based on support vector machine for regression and genetic algorithms using acoustic emission. Journal of Vibration Engineering & Technologies, 7, 455-464, 2019. https://doi.org/10.1007/s42417-019-00143-y

[9] B.R.F. Rende, A.A. Cavalini Jr and I.F. Santos, Fault detection using vibration data-driven models—a simple and well-controlled experimental example. Journal of the Brazilian Society of Mechanical Sciences and Engineering, 44(6), 229, 2022. https://doi.org/10.1007/s40430-022-03462-6

[10] H. Wang and P. Chen, A feature extraction method based on information theory for fault diagnosis of reciprocating machinery. Sensors, 9(4), 2415-2436, 2009. https://doi.org/10.3390/s90402415

[11] C. Malla and I. Panigrahi, Review of condition monitoring of rolling element bearing using vibration analysis and other techniques. Journal of Vibration Engineering & Technologies, 7, 407-414, 2019. https://doi.org/10.1007/s42417-019-00119-y

[12] S.K. Gundewar and P.V. Kane, Condition monitoring and fault diagnosis of induction motor. Journal of Vibration Engineering & Technologies, 9, 643-674, 2021. https://doi.org/10.1007/s42417-020-00253-y

[13] Q. He, Y. Liu, Q. Long and J. Wang, Time-frequency manifold as a signature for machine health diagnosis. IEEE Transactions on Instrumentation and Measurement, 61(5), 1218-1230, 2012. https://doi.org/10.1109/TIM.2012.2183402

[14] H. Cao, F. Fan, K. Zhou and Z. He, Wheel-bearing fault diagnosis of trains using empirical wavelet transform. Measurement, 82, 439-449, 2016. https://doi.org/10.1016/j.measurement.2016.01.023

[15] Y. Gao, D. Yu and H. Wang, Fault diagnosis of rolling bearings using weighted horizontal visibility graph and graph Fourier transform. Measurement, 149, 107036, 2020. https://doi.org/10.1016/j.measurement.2019.107036

[16] D. Zhao, W. Cheng, R.X. Gao, R. Yan and P. Wang, Generalized Vold–Kalman filtering for nonstationary compound faults feature extraction of bearing and gear. IEEE Transactions on Instrumentation and Measurement, 69(2), 401-410, 2019. https://doi.org/10.1109/TIM.2019.2903700

[17] B. Muruganatham, M.A. Sanjith, B. Krishnakumar and S.S. Murty, Roller element bearing fault diagnosis using singular spectrum analysis. Mechanical systems and signal processing, 35(1-2), 150-166, 2013. https://doi.org/10.1016/j.ymssp.2012.08.019

[18] J.B. Ali, N. Fnaiech, L. Saidi, B. Chebel-Morello and F. Fnaiech, Application of empirical mode decomposition and artificial neural network for automatic bearing fault diagnosis based on vibration signals. Applied Acoustics, 89, 16-27, 2015. https://doi.org/10.1016/j.apacoust.2014.08.016

[19] Y. Li, Q. Gao, B. Miao, W. Zhang, J. Liu and Y. Zhu, Application of the refined multiscale permutation entropy method to fault detection of rolling bearing. Journal of the Brazilian Society of Mechanical Sciences and Engineering, 43(5), 280, 2021. https://doi.org/10.1007/s40430-021-02986-7

[20] Y. Cheng, S. Wang, B. Chen, G. Mei, W. Zhang, H. Peng and G. Tian, An improved envelope spectrum via candidate fault frequency optimization-gram for bearing fault diagnosis. Journal of Sound and Vibration, 523, 116746, 2022. https://doi.org/10.1016/j.jsv.2022.116746

[21] Y. Wang and M. Liang, Identification of multiple transient faults based on the adaptive spectral kurtosis method. Journal of Sound and Vibration, 331(2), 470-486, 2012. https://doi.org/10.1016/j.jsv.2011.08.029

[22] J.K. Alsalaet, Fast averaged cyclic periodogram method to compute spectral correlation and coherence. ISA transactions, 129, 609-630, 2022. https://doi.org/10.1016/j.isatra.2022.01.029

[23] Z. Feng, H. Ma and M.J. Zuo, Spectral negentropy based sidebands and demodulation analysis for planet bearing fault diagnosis. Journal of Sound and

Vibration, 410, 124-150, 2017. https://doi.org/10.1016/j.jsv.2017.08.024

[24] D. Wang, X. Zhao, L.L. Kou, Y. Qin, Y. Zhao and K.L. Tsui, A simple and fast guideline for generating enhanced/squared envelope spectra from spectral coherence for bearing fault diagnosis. Mechanical Systems and Signal Processing, 122, 754-768, 2019. https://doi.org/10.1016/j.ymssp.2018.12.055

[25] B. Tang, W. Liu and T. Song, Wind turbine fault diagnosis based on Morlet wavelet transformation and Wigner-Ville distribution. Renewable Energy, 35(12), 2862-2866, 2010. https://doi.org/10.1016/j.renene.2010.05.012

[26] W. Sun, G. An Yang, Q. Chen, A. Palazoglu and K. Feng, Fault diagnosis of rolling bearing based on wavelet transform and envelope spectrum correlation. Journal of Vibration and Control, 19(6), 924-941, 2013. https://doi.org/10.1177/1077546311435348

[27] F. Zou, H. Zhang, S. Sang, X. Li, W. He and X. Liu, Bearing fault diagnosis based on combined multi-scale weighted entropy morphological filtering and bi-LSTM. Applied Intelligence, 1-18, 2021. https://doi.org/10.1007/s10489-021-02229-1

[28] Z. Feng, D. Zhang and M. J. Zuo, Adaptive mode decomposition methods and their applications in signal analysis for machinery fault diagnosis: a review with examples. IEEE access, 5, 24301-24331, 2017. https://doi.org/10.1109/ACCESS.2017.2766232

[29] W. Ying, J. Tong, Z. Dong, H. Pan, Q. Liu and J. Zheng, Composite multivariate multi-Scale permutation entropy and laplacian score based fault diagnosis of rolling bearing. Entropy, 24(2), 160, 2022. https://doi.org/10.3390/e24020160

[30] J. Altmann and J. Mathew, Multiple band-pass autoregressive demodulation for rolling-element bearing fault diagnosis. Mechanical systems and signal processing, 15(5), 963-977, 2001. https://doi.org/10.1006/mssp.2001.1410

[31] C. Xu, C. Wang and Liu, Nonstationary vibration signal analysis using Wavelet-based time–frequency filter and wigner–ville distribution. Journal of Vibration and Acoustics, 138(5), 051009, 2016. https://doi.org/10.1115/1.4033641

[32] H. Ramoser, J. Muller-Gerking, and G. Pfurtscheller, Optimal spatial filtering of single trial EEG during imagined hand movement. IEEE transactions on rehabilitation engineering, 8(4), 441-446, 2000. https://doi.org/%2010.1109/86.895946

[33] I. Xygonakis, A. Athanasiou, N. Pandria, D. Kugiumtzis and P.D. Bamidis, Decoding motor imagery through common spatial pattern filters at the EEG source space. Computational intelligence and neuroscience, ID 7957408, 2018. https://doi.org/10.1155/2018/7957408

[34] Y.E. Karabacak and N.G. Özmen, Common spatial pattern-based feature extraction and worm gear fault detection through vibration and acoustic measurements. Measurement, 187, 110366, 2022. https://doi.org/10.1016/j.measurement.2021.110366

[35] Z. Li, Y. Lv, R. Yuan and Q. Zhang, An intelligent fault diagnosis method of rolling bearings via variational mode decomposition and common spatial pattern-based feature extraction. IEEE Sensors Journal, 22(15), 15169-15177, 2022. https://ieeexplore.ieee.org/document/9807645

[36] Case Western Reserve University Bearing Data Center Website. http://csegroups.case.edu/bearingdatacenter, Accessed 14.7.2023

[37] R.B. Randall, Vibration-based condition monitoring: industrial, automotive and aerospace applications. John Wiley & Sons, NJ, 2021.

[38] A. Gabrielli, M. Battarra, E. Mucchi and G. Dalpiaz, Acceleration signals of rolling element bearings with artificial defects. Mendeley Data, 2022. https://doi.org/10.17632/8wdzm5gwng.1

[39] P. Kumar and A.S. Hati, Review on machine learning algorithm based fault detection in induction motors. Archives of Computational Methods in Engineering, 28, 1929-1940, 2021. https://doi.org/10.1007/s11831-020-09446-w

[40] T. Han, D. Jiang, Q. Zhao, L. Wang and K. Yin, Comparison of random forest, artificial neural networks and support vector machine for intelligent diagnosis of rotating machinery. Transactions of the Institute of Measurement and Control, 40(8), 2681-2693, 2018. https://doi.org/10.1177/0142331217708242

[41] L.B. Jack and A.K. Nandi, Fault detection using support vector machines and artificial neural networks, augmented by genetic algorithms. Mechanical systems and signal processing, 16(2-3), 373-390, 2002. https://doi.org/10.1006/mssp.2001.1454

[42] S. Liu, J. Xie, C. Shen, X. Shang, D. Wang and Zhu, Z, Bearing fault diagnosis based on improved convolutional deep belief network. Applied Sciences, 10(18), 6359, 2020. https://doi.org/10.3390/app10186359

[43] R. Liu, B. Yang, E. Zio and X. Chen, Artificial intelligence for fault diagnosis of rotating machinery: A review. Mechanical Systems and Signal Processing, 108, 33-47, 2018. https://doi.org/10.1016/j.ymssp.2018.02.016

[44] H. Zhao, X. Yang, B. Chen, H. Chen and W. Deng, Bearing fault diagnosis using transfer learning and optimized deep belief network. Measurement Science and Technology, 33(6), 065009, 2022. https://doi.org/10.1088/1361-6501/ac543a

[45] Y. Kaya, M. Kuncan, K. Kaplan, M.R. Minaz and H.M. Ertunç, A new feature extraction approach based on one dimensional gray level co-occurrence matrices for bearing fault classification. Journal of Experimental & Theoretical Artificial Intelligence, 33(1), 161-178, 2021. https://doi.org/10.1080/0952813X.2020.1735530

[46] S. Bayram, K. Kaplan, M. Kuncan and H. M. Ertunç, The effect of bearings faults to coefficients obtaned by using wavelet transform. 22nd Signal Processing and

Communications Applications Conference (SIU), pp. 991-994, Trabzon, Turkey, 23-25 April 2014.

[47] Y. Kaya, F. Kuncan and H.M. Ertunç, A new automatic bearing fault size diagnosis using time-frequency images of CWT and deep transfer learning methods. Turkish Journal of Electrical Engineering and Computer Sciences, 30(5), 1851-1867, (2022). https://doi.org/10.55730/1300-0632.3909

[48] M. Kuncan, An Intelligent Approach for Bearing Fault Diagnosis: Combination of 1D-LBP and GRA. IEEE Access, 8, 137517-137529, 2020. https://doi.org/10.1109/ ACCESS.2020.3011980.

[49] H. Yang, X. Li and W. Zhang, Interpretability of deep convolutional neural networks on rolling bearing fault diagnosis. Measurement Science and Technology, 33(5), 055005, 2022. https://doi.org/10.1088/1361-6501/ac41a5

[50] N.M. Thoppil, V. Vasu and C.S.P. Rao, Deep learning algorithms for machinery health prognostics using time-series data: A review. Journal of Vibration Engineering & Technologies, 1-23, 2021. https://doi.org/10.1007/s42417-021-00286-x

[51] W.A. Smith and R.B. Randall, Rolling element bearing diagnostics using the Case Western Reserve University data: A benchmark study. Mechanical systems and signal processing, 64, 100-131, 2015. https://doi.org/10.1016/j.ymssp.2015.04.021

[52] H. Nguyen-Schäfer, Computational design of rolling bearings. Springer International Publishing, Cham, 2016.

[53] T. Nguyen, I. Hettiarachchi, A. Khatami, L. Gordon-Brown, C.P. Lim and S. Nahavandi, Classification of multi-class BCI data by common spatial pattern and fuzzy system. IEEE access, 6, 27873-27884, 2018. https://doi.org/10.1109/ACCESS.2018.2841051

[54] V. Martínez-Cagigal, Common Spatial Patterns (CSP), MATLAB Central File Exchange. https://www.mathworks.com/matlabcentral/fileexchange/72204-common-spatial-patterns-csp, Accessed 14.07.2023.

[55] Y.E. Karabacak, N.G. Özmen and L. Gümüşel, Intelligent worm gearbox fault diagnosis under various working conditions using vibration, sound and thermal features. Applied Acoustics, 186, 108463, 2022. https://doi.org/10.1016/j.apacoust.2021.108463

[56] D.J. Bordoloi and R. Tiwari, Optimum multi-fault classification of gears with integration of evolutionary and SVM algorithms. Mechanism and Machine Theory, 73, 49-60, 2014. https://doi.org/10.1016/j.mechmachtheory.2013.10.006

[57] Q. Wang, S. Wang, B. Wei, W. Chen and Y. Zhang, Weighted K-NN classification method of bearings fault diagnosis with multi-dimensional sensitive features. IEEE Access, 9, 45428-45440, 2021. https://doi.org/10.1109/ACCESS.2021.3066489

[58] A.A.A. Mohd Amiruddin, H. Zabiri, S.A.A. Taqvi and L.D. Tufa, Neural network applications in fault diagnosis and detection: an overview of implementations in engineering-related systems. Neural Computing and Applications, 32, 447-472, 2020. https://doi.org/10.1007/s00521-018-3911-5

[59] Y. Bengio and Y. LeCun, Scaling Learning Algorithms towards AI. in: L. Bottou, O. Chapelle, D. DeCoste, J. Weston (Eds.), Large-Scale Kernel Machines, MIT Press, NY, 2007.

[60] Z. Xia, S. Xia, L. Wan and S. Cai, Spectral regression based fault feature extraction for bearing accelerometer sensor signals. Sensors, 12(10), 13694-13719, 2012. https://doi.org/10.3390/s121013694

[61] J. Sun, C. Yan and J. Wen, Intelligent bearing fault diagnosis method combining compressed data acquisition and deep learning. IEEE Transactions on Instrumentation and Measurement, 67(1), 185-195 2017. https://doi.org/10.1109/TIM.2017.2759418

[62] M. Sun, Z. Song, X. Jiang, J. Pan and Y. Pang, Learning pooling for convolutional neural network. Neurocomputing, 224, 96-104, 2017. https://doi.org/10.1016/j.neucom.2016.10.049

[63] Y.E. Karabacak and N. Gürsel Özmen, Application of Deep Learning Method for Condition Monitoring and Fault Diagnosis from Vibration Data in Bearings. Konya Journal of Engineering Sciences, 10(2), 346-365, 2022. https://doi.org/10.36306/konjes.1049489